Graph-Based Interpolation of Local Activation Time on the Cardiac Surface

Jennifer Hellar*, Romain Cosentino*, Mathews M John†, Allison Post†, Skylar Buchan†,
Mehdi Razavi‡, Behnaam Aazhang*
*Department of Electrical and Computer Engineering, Rice University
†Electrophysiology Clinical Research and Innovations, Texas Heart Institute
‡Department of Cardiology, Texas Heart Institute

***Abstract*—We propose a novel method for spatial interpolation of local activation times (LATs), a feature extracted from intracardiac electrograms (EGMs) which are sampled at various points of interest on the heart. Cardiologists utilize the projection of the LAT signal onto a 3D visualization of the heart to aid in determining the effects of intervention or the source of arrhythmias during cardiac ablation procedures. For an accurate and complete LAT map, technicians must record at many locations, a slow process which results in samples that are still sparse due to time constraints and must be interpolated to estimate the feature value over the entire surface. The method proposed here utilizes a graph signal processing framework to reformulate the irregular spatial interpolation problem into a semi-supervised learning problem with a closed-form solution. The method is evaluated on a patient dataset obtained by the CARTO electroanatomic mapping system during a premature ventricular complex (PVC) ablation procedure. Our approach outperforms standard interpolation techniques, resulting in a 2x higher signal-to-noise ratio (SNR).**

I. Introduction

Cardiac arrhythmias, or irregularities in the heart's normal rhythm, contributed to more than 550,000 deaths in the US in 2017 [1]. One of the most common treatments for a variety of cardiac arrhythmias, including supraventricular tachycardias, atrial fibrillation, and many forms of ventricular tachycardia, is cardiac ablation; between 2000 and 2013, an estimated 519,951 ablation procedures were performed [2]. During an ablation procedure, a cardiologist inserts catheters through the veins of the patient into the heart and burns the tissues responsible for triggering the arrhythmia, thereby terminating the abnormal activation [3].

In each procedure, ablation target(s) are predominantly identified by examination of a 3D rendering of the Local Activation Time (LAT) signal on the surface of the cardiac tissue as in Fig. 1, called an LAT map. The LAT map characterizes the spread of the electrical activation wave within the cardiac chamber, allowing physicians to visualize the electrical propagation [4]. After each ablation, a new LAT map is generated to view the effect of the intervention and identify further ablation targets. Methods for obtaining the LAT samples and for interpreting the LAT map have been prominently discussed in the medical literature for some time already [4]–[6].

LAT samples are extracted from local electrogram (EGM) signals recorded from the cardiac surface. One characteristic signal feature is selected as a reference, and the difference in time between the appearance of that feature in the EGM at each recorded location (t_i) and in the reference t_0 is the local activation time $LAT_i = t_i - t_0$. Once a sufficient number of samples has been collected, they are interpolated to approximate the true, smooth signal on the surface.

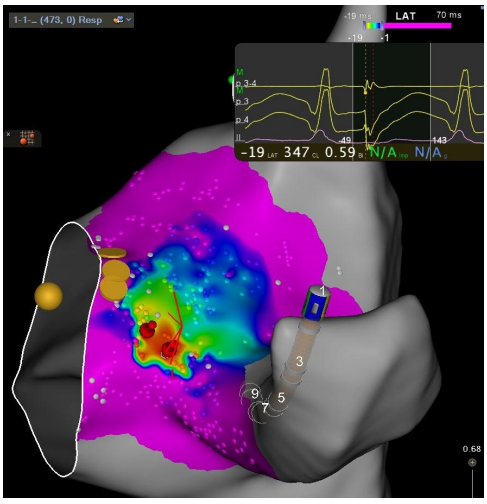

Fig. 1. A typical LAT map (3D rendering of the LAT signal) where small dots represent LAT sample points and color encodes the LAT value, with red being earliest activation and purple being latest.

Presently, for an accurate interpolation, technicians will record dozens and sometimes hundreds of locations on the surface, a process which significantly increases the overall ablation procedure time since a new map has to be generated after each attempted ablation. The problem of LAT interpolation therefore remains an open and critical research question.

Only a few groups have even attempted to address this problem [7]–[9]. These works focus on LAT interpolation via cubic spline interpolation [7], radial basis functions of Cartesian distances [8] or Gaussian processes [9]. The drawback of these approaches, however, is that they either do not take into account the underlying surface geometry [7], [8] or else assume a Gaussian prior on some transformation of the data [9].

To address these issues, we propose to use graph signal processing to perform LAT interpolation utilizing the manifold

geometry. It will be shown that this method follows from an intuitive re-formulation of the interpolation problem which incorporates key results in the fields of graph signal processing [10], [11] and geometric learning [12]–[14].

The paper is organized as follows. Section II describes the dataset used for testing and analysis of this method. Section III outlines the mathematical framework of our graph-based approach. Section IV evaluates the performance of our method on the patient dataset. Sections V and VI discuss the results and the interpretation.

II. Dataset

Our dataset consists of a representative patient LAT map obtained by the CARTO electroanatomic mapping system during a premature ventricular complex (PVC) ablation procedure. This map is comprised of

1) A triangular mesh approximating the anatomy of the cardiac chamber, provided in Biosense Webster Triangulated Mesh file format. The triangular mesh $\{\mathcal{V}, \mathcal{F}\}$ approximates the geometry of the surface with
   a) $\mathcal{V}$, an ordered set of vertices $v_i \in \mathbb{R}^3$ for $i = 1, 2, ..., n$ which are locations on the cardiac surface, and
   b) $\mathcal{F} \subset \mathcal{V} \times \mathcal{V} \times \mathcal{V}$, a set of triangular faces where a face $(v_i, v_j, v_k) \in \mathcal{F}$ defines edges between the three vertices v_i, v_j, and $v_k \in \mathcal{V}$.
2) A set of LAT sample values $s_1, ..., s_m$ and corresponding locations in $\mathbb{R}^3$. Note that the sample locations do not always coincide with a vertex of the mesh.

This dataset map contains $n = 6376$ mesh vertices with $m = 867$ LAT samples. It has one interesting feature, a sizable spatial region of drastic signal variation which is visible in Fig. 2a, where vertices with very low LAT values (e.g. -200ms) are adjacent to vertices with high LAT values (e.g. $+50$ms). This "early-meets-late" phenomenon can occur in patients with macro re-entrant circuits overriding the natural sinus rhythm and causing arrhythmia. It can also occur when the reference for measuring local activation time is changed or disturbed, so that some LAT samples are measured relative to a different reference. In either case, a good interpolation which captures the high-frequency content of this sharp transition is still required.

III. Methods

Let $\mathcal{M}$ be the smooth manifold that is the surface of the heart. In general, we want an interpolant function $f : \mathcal{M} \to \mathbb{R}$ which maps any location on the manifold to its LAT value such that the function generalizes to the whole manifold. In our dataset, the triangular mesh $\{\mathcal{V}, \mathcal{F}\}$ approximates the manifold $\mathcal{M}$ so we instead pursue a discrete interpolant function $f : \mathcal{V} \to \mathbb{R}$ which outputs the LAT value for any vertex $v_i \in \mathcal{V}$.

A. LAT signal pre-processing

Due to measurement imprecision, LAT sample coordinates do not exactly coincide with vertex coordinates in $\mathcal{V}$. To process the signal on the surface, we assign each LAT value $s_1, ..., s_m$ to the nearest surface vertex in $\mathcal{V}$, giving us a subset of sampled vertices $\mathcal{V}_\mathcal{S}$.

TABLE I
Summary of key notations.

Notation	Definition
a, **a**, **A**	Scalar, vector, matrix
$\mathbb{R}^n$	n-dimensional Euclidean space
$\mathcal{V}, \mathcal{E}, \mathcal{F}$	Vertices and edges of a graph, faces of a mesh $\mathcal{V} \subset \mathbb{R}^3$, $\mathcal{E} \subset \mathcal{V} \times \mathcal{V}$, $\mathcal{F} \subset \mathcal{V} \times \mathcal{V} \times \mathcal{V}$
$w_{ij}, \mathbf{W}$	Adjacency matrix of a graph
$\mathbf{L}$	Unnormalized graph Laplacian
$\mathbf{f}$	LAT function/signal on vertices of a graph
$\hat{\mathbf{f}}$	Fourier transform of $\mathbf{f}$
$\mathcal{V}_\mathcal{S}$	Set of sampled graph vertices $\mathcal{V}_\mathcal{S} \subset \mathcal{V}$
$\mathbf{f_s}$	Partially sampled LAT signal
n	Number of vertices, $\lvert\mathcal{V}\rvert$
m	Number of LAT samples, $\lvert\mathcal{V}_\mathcal{S}\rvert$

B. Graph construction

We transform the mesh into an undirected graph $\mathcal{G} = \{\mathcal{V}, \mathcal{E}, \mathbf{W}\}$ such that the set of vertices $\mathcal{V}$ with $|\mathcal{V}| = n$ is unchanged. An edge (v_i, v_j) is included in the set of edges $\mathcal{E}$ if and only if v_i and v_j form two corners of a face in $\mathcal{F}$. The $n \times n$ adjacency matrix $\mathbf{W}$ has entries w_{ij} given by

$$w_{ij} = \begin{cases} 1 & (v_i, v_j) \in \mathcal{E} \\ 0 & \text{otherwise.} \end{cases}$$

Our interpolant function $f : \mathcal{V} \to \mathbb{R}$ is a graph signal defined on the vertices of the graph and represented as a vector $\mathbf{f} \in \mathbb{R}^n$ where the i^{th} component of vector $\mathbf{f}$ represents the function value at the i^{th} vertex in $\mathcal{V}$. Our partially sampled LAT graph signal $\mathbf{f_s} \in \mathbb{R}^n$ then has non-zero values only for vertices in the sampled set,

$$f_s(v_i) = \begin{cases} s_i & v_i \in \mathcal{V}_\mathcal{S} \\ 0 & \text{otherwise.} \end{cases}$$

Letting $\mathbf{D}$ be the diagonal degree matrix of $\mathcal{G}$, we compute the unnormalized graph Laplacian,

$$\mathbf{L} = \mathbf{D} - \mathbf{W},$$

which forms a real symmetric matrix that encapsulates the connectivity of $\mathcal{G}$. For further information regarding this particular operator, refer to [15].

Note that this graph $\mathcal{G}$ is purely mesh-based and does not contain any information about the possible causes for high-frequency LAT signal variation (scar tissue blocking electrical activation, opposite edges of a reentrant cycle meeting, etc.). Therefore, we also implement graph $\mathcal{G}^* = \{\mathcal{V}, \mathcal{E}^*, \mathbf{W}^*\}$ which removes functional connections (edges) that are not physiologically present for one of those reasons. To do this, we

compute a quantization of the manifold using Nearest Neighbors (NN) applied onto the LAT signal. From this quantization, we are able to remove any graph edges $(v_i, v_j) \in \mathcal{E}$ with a $\Delta LAT_{ij} \geq 50$ms, resulting in a sparsified graph that is a more descriptive representation of the physiological manifold.

C. Re-formulating the interpolation problem

Our graph construction defines a sampling of the manifold $\mathcal{M}$ at the graph vertices $\mathcal{V}$, with a corresponding discrete spatial sampling $\mathbf{f} = [s_1, ..., s_n]^T$ of the underlying continuous LAT signal. Since we do not have a complete signal $\mathbf{f}$, we want to estimate it with $\mathbf{f}^*$, a smooth interpolation of the partially sampled signal $\mathbf{f_s}$. To do this, we solve the following optimization problem,

$$\mathbf{f}^* = \arg\min_{\mathbf{f}\in\mathbb{R}^n} ||\mathbf{M_l}(\mathbf{f} - \mathbf{f_s})||_2^2 + \alpha||\mathbf{M_u}\mathbf{f}||_2^2 + \beta\mathbf{f}^T\mathbf{L}\mathbf{f}. \quad (1)$$

Here, the first term is signal assignment loss with $\mathbf{M_l}$ a diagonal binary matrix corresponding to labelled (known) samples $s_1, ..., s_m$. The second term is a standard Tikhonov regularization to reduce the magnitude of unknown samples selected by the diagonal binary matrix $\mathbf{M_u}$. Note that $\mathbf{M_l} + \mathbf{M_u} = \mathbf{I}$, the $n \times n$ identity matrix. The third term, a Dirichlet regularization, ensures signal smoothness; it is the weighted sum of adjacent signal differences squared,

$$\mathbf{f}^T\mathbf{L}\mathbf{f} = \frac{1}{2}\sum_{i,j=1}^{n} w_{ij}(f_i - f_j)^2.$$

This manifold regularization approach has been developed and studied in graph signal processing literature for some time (see [11], [12]), but not in the context of this application. The solution to (1), for which the proof is omitted for brevity, is

$$\mathbf{f}^* = (\mathbf{M_l} + \alpha\mathbf{M_u} + \beta\mathbf{L})^{-1}\mathbf{f_s}. \quad (2)$$

For our application, optimal regularization coefficients $\alpha = 0.001$ and $\beta = 1.0$ were obtained during cross-validation over values

$$\alpha = [10^{-5}, 10^{-4}, 10^{-3}, 10^{-2}, 10^{-1}, 1, 10, 10^2, 10^3],$$

$$\beta = [10^{-2}, 10^{-1}, 1, 2, 4, 5, 8, 10, 10^2, 10^3].$$

In particular, further increasing β, the coefficient of smoothing, did not significantly change the interpolation performance, but reducing it resulted in consistently higher error. Intuitively, we expect a certain level of smoothness in the signal which this parameter captures.

Interestingly, the expression in (2) which gives us our semi-supervised learning solution may also be viewed from a filtering perspective which we discuss in Section V. The solution in (2) is hereafter referred to as MAGIC-LAT (Manifold-Approximating Graph Interpolation for Cardiac LAT).

TABLE II
PERFORMANCE COMPARISON VERSUS STANDARD ALGORITHMS

	NMSE	SNR
Nearest Neighbor Interpolation	0.53 ± 0.015	5.47 ± 0.253
GPR Interpolation	0.31 ± 0.002	10.13 ± 0.068
MAGIC-LAT (our)	$\mathbf{0.30 \pm 0.002}$	$\mathbf{10.36 \pm 0.057}$
MAGIC-LAT, sparsified (our)	$\mathbf{0.06 \pm 0.004}$	$\mathbf{24.41 \pm 0.587}$

IV. RESULTS

Our results are organized as follows. Section IV-A describes the naive application of MAGIC-LAT to interpolate the patient LAT map using the full graph $\mathcal{G}$. Section IV-B then demonstrates the true capability of MAGIC-LAT by interpolating on the sparsified graph $\mathcal{G}^*$. We further evaluate the performance of MAGIC-LAT in Section IV-C by varying the number of training samples used for interpolation.

A. MAGIC-LAT on $\mathcal{G}$, $m/n = 12\%$ sampling

We use m =780 LAT samples as our training input $\mathbf{f_s}$ (12% of the total ~6400 vertices). Since we only have ground truth for 867 vertices, we perform cross-validation on these, selecting a unique random test set of 87 known vertices to estimate for each fold of the cross-validation. Individual estimates for each fold are aggregated into an overall graph-estimated signal, shown in Fig. 2b. This process is repeated 5x to capture error mean and variance.

In the smooth regions on the right and left sides of the image, the interpolation estimate on $\mathcal{G}$ closely approximates the ground truth values. Across the high-frequency region, however, our method incorrectly estimates a smooth gradient of LAT values rather than the true sharp transition. Intuitively, MAGIC-LAT linearly propagates the recorded LAT samples with respect to the heart surface as captured by the graph connectivity. The purely mesh-based graph $\mathcal{G}$ includes false functional connections across the high-frequency region, resulting in an incorrect local signal estimate.

B. MAGIC-LAT on sparsified $\mathcal{G}^*$, $m/n = 12\%$ sampling

With the same test setup as the previous experiment, we apply MAGIC-LAT to the sparsified graph $\mathcal{G}^*$, which excludes the false functional connections in $\mathcal{G}$. The estimated signal after interpolation on $\mathcal{G}^*$ is shown in Fig. 2c. Here, our interpolation almost perfectly approximates the ground truth signal.

Our results for both experiments are summarized in Table II. Compared to standard interpolation algorithms, our method achieves 5x lower normalized mean squared error (NMSE) and 2x higher signal-to-noise ratio (SNR). NMSE and SNR are defined for an arbitrary signal $\mathbf{y}$ with mean $\mu_\mathbf{y}$ and estimate $\mathbf{y}^*$ as

$$NMSE = \frac{||\mathbf{y}^* - \mathbf{y}||_2^2}{||\mathbf{y} - \mu_\mathbf{y}||_2^2}, \quad SNR = 20log_{10}(NMSE^{-1}).$$

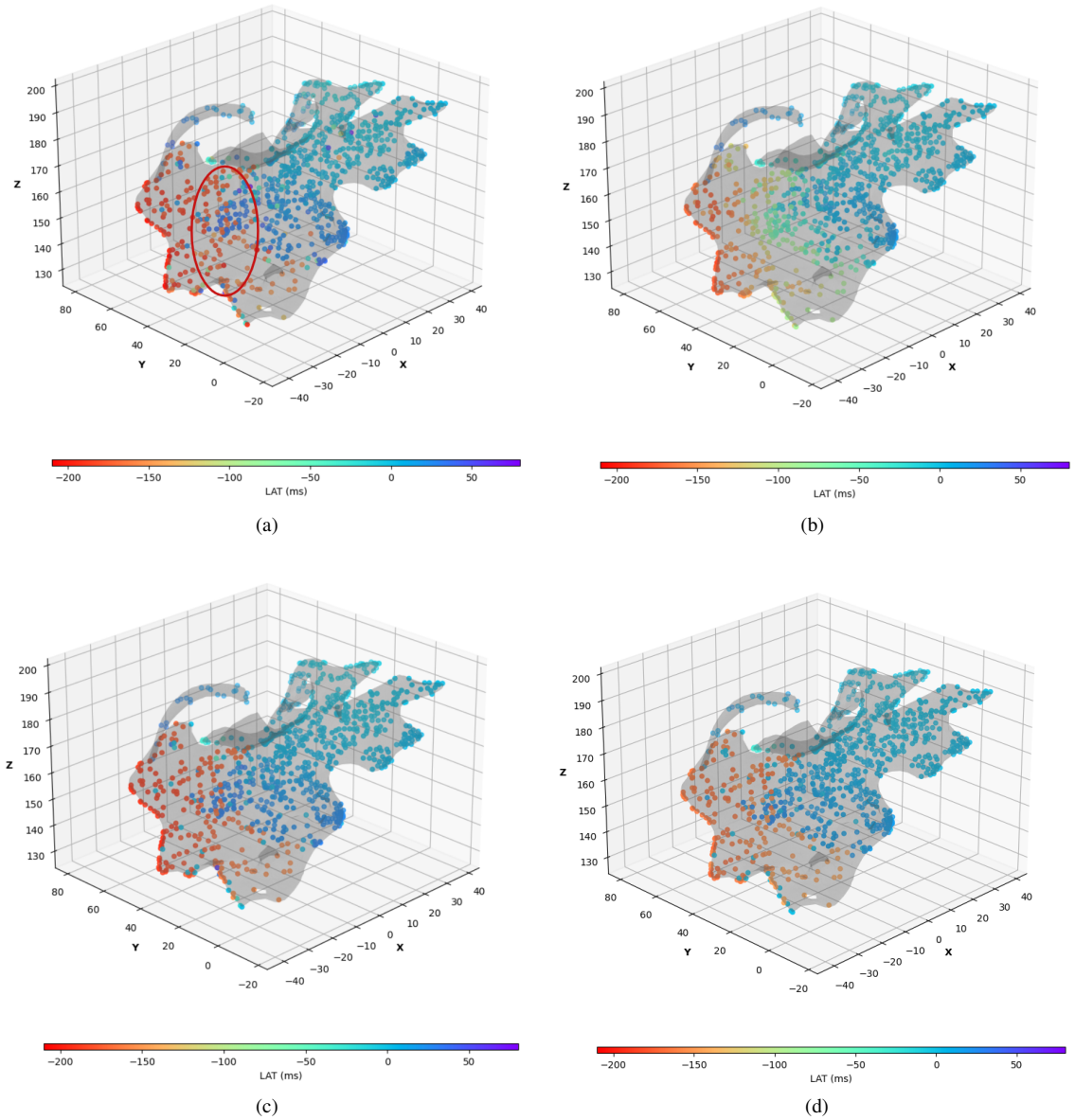

(a) (b) (c) (d)

Fig. 2. (a) Ground truth contains a region of high-frequency variation which is circled in red. (b) The interpolation reconstructed signal on the purely mesh-based graph $\mathcal{G}$ is accurate except for values in the high-frequency region. (c) The interpolation reconstructed signal on the sparsified graph $\mathcal{G}^*$ almost perfectly approximates the ground truth. (d) The interpolation reconstructed signal (on $\mathcal{G}^*$) based on only 1.4% of the vertices is still visually similar to ground truth.

For Gaussian Process Regression (GPR), we use a kernel sum of three radial basis functions with length scales of 0.01, 0.1, and 1.

C. MAGIC-LAT on sparsified $\mathcal{G}^*$, varied sampling

We now vary m, the number of input training samples, from $87 - 824$ vertices ($\sim 1.4 - 13\%$ of the total vertices) with the results given in Fig. 3. We see that our method maintains very low interpolation error when at least 10% of the vertices are sampled. Even when only 1.4% of the mesh is sampled, we can reconstruct a reasonable signal but have difficulty estimating values at the extremes of the LAT range as seen in Fig. 2d.

V. Discussion

A. Interpreting our graph-based solution

To interpret our method, we consider the case where $\alpha = \beta = 1$ and substitute the spectral decomposition of the Laplacian $\mathbf{L} = \mathbf{U}\mathbf{\Lambda}\mathbf{U}^T$ to re-write (2) as

$$\mathbf{f}^* = \mathbf{U}(\mathbf{I} + \mathbf{\Lambda})^{-1}\mathbf{U}^T\mathbf{f_s}. \tag{3}$$

To analyze (3), we recall that in Euclidean space, the Laplace operator denoted as ∇^2, is defined as the divergence of the gradient and is given by the sum of all unmixed second partial derivatives, $\nabla^2 f = \sum_i \frac{\partial^2 f}{\partial x_i^2}$, for Cartesian coordinates x_i.

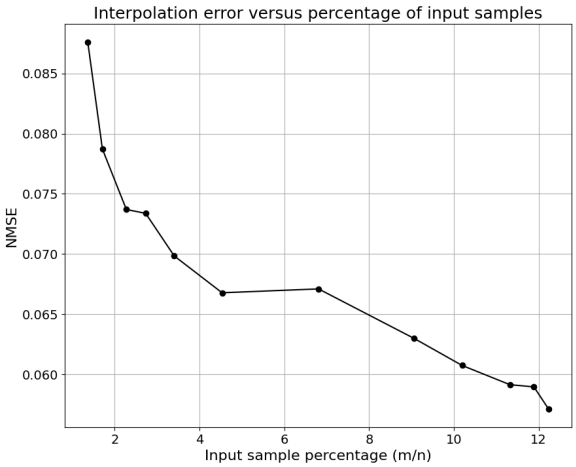

Fig. 3. Interpolation error for various signal sampling percentages (m/n). The interpolation is repeated 5x for each m and the mean error reported.

The Laplacian appears in differential equations describing heat diffusion, wave propagation, and other physical phenomena governed by second-order mechanics. We see that eigenfunctions of the Laplacian form a Fourier basis since we have

$$\nabla^2 e^{2\pi i w t} = -(2\pi w)^2 e^{2\pi i w t}.$$

The generalization of the Laplacian to functions defined on Riemannian manifolds is the Laplace-Beltrami operator. Interestingly, the graph Laplacian converges to the Laplace-Beltrami operator under certain conditions (see [13], [14]), and Laplacian eigenvectors therefore form a good approximation of a Fourier basis on the manifold. This gives us the notion of a Fourier transform of a graph signal given by $\hat{\mathbf{f}} = \mathbf{U}^T\mathbf{f}$ with inverse transform $\mathbf{f} = \mathbf{U}\hat{\mathbf{f}}$. By extension, a general filtration of $\mathbf{f}$ with filter $\mathbf{h}$ is

$$\mathbf{f_{filt}} = \mathbf{U}\hat{\mathbf{h}}(\mathbf{\Lambda})\mathbf{U}^T\mathbf{f}, \tag{4}$$

where $\hat{\mathbf{h}}(\mathbf{\Lambda}) = diag(\hat{h}(\lambda_1), ..., \hat{h}(\lambda_n))$ is the spectral representation of the filter [10].

Comparing (3) with (4), we immediately observe that our interpolation solution is the output of a filter on our input signal $\mathbf{f_s}$ with the particular filter $\hat{\mathbf{h}}(\mathbf{\Lambda}) = (\mathbf{I} + \mathbf{\Lambda})^{-1}$ determined by our optimization formulation. This interpolation via filtering is a novel perspective and motivates further investigation into other filter constructions.

B. Revisiting the local high-frequency region

The difficulty of interpolating the local high-frequency content of the LAT signal motivates another interesting conclusion. It is well understood that time-frequency localized transforms like the wavelet transform outperform the Fourier basis for processing signals that are localized in both domains. This suggests that a spatially-localized graph filter may provide an accurate interpolation even in high-frequency regions, perhaps without the graph structure sparsification we have proposed here.

VI. Conclusion

We proposed and validated a novel method for spatial interpolation of the local activation time (LAT) signal derived during cardiac ablation procedures. We demonstrated that our method, MAGIC-LAT, accurately reconstructs a smooth LAT signal when only $\sim$10% of the mesh is sampled and outperforms existing techniques. Our method provides cardiologists with an accurate and complete estimate of the true local activation time map based on relatively few measurements. Beyond its capability, we also describe how, through the lens of filtering, we can extend our approach to better characterize electrical activation propagation and spatial localization in cardiac tissue. In future work, this method will be extended to more patients and different LAT maps.

References

[1] S. S. Virani, A. Alonso, E. J. Benjamin, M. S. Bittencourt, C. W. Callaway, A. P. Carson, A. M. Chamberlain, A. R. Chang *et al.*, "Heart disease and stroke statistics—2020 update: a report from the american heart association," *Circulation*, vol. 141, no. 9, pp. e139–e596, 2020.

[2] S. Hosseini, G. Rozen, A. Saleh, J. Vaid *et al.*, "Catheter ablation for cardiac arrhythmias," *JACC: Clinical Electrophysiology*, vol. 3, no. 11, pp. 1240–1248, 2017.

[3] M. D. Lesh, G. F. Van Hare, L. M. Epstein, A. P. Fitzpatrick, M. M. Scheinman, R. J. Lee, M. A. Kwasman, H. R. Grogin, and J. C. Griffin, "Radiofrequency catheter ablation of atrial arrhythmias. results and mechanisms." *Circulation*, vol. 89, no. 3, pp. 1074–1089, 1994.

[4] C. Cantwell, C. Roney, F. Ng, J. Siggers, S. Sherwin, and N. Peters, "Techniques for automated local activation time annotation and conduction velocity estimation in cardiac mapping," *Computers in Biology and Medicine*, vol. 65, pp. 229–242, 2015.

[5] N. de Groot, M. Schalij, K. Zeppenfeld, N. Blom, E. Van der Velde *et al.*, "Voltage and activation mapping: how the recording technique affects the outcome of catheter ablation procedures in patients with congenital heart disease," *Circulation*, vol. 108, no. 17, pp. 2099–2106, 2003.

[6] J. Acosta, D. Soto-Iglesias, J. Fernández-Armenta, M. Frutos-López, B. Jáuregui *et al.*, "Clinical validation of automatic local activation time annotation during focal premature ventricular complex ablation procedures," *Ep Europace*, vol. 20, no. FI2, pp. f171–f178, 2018.

[7] B. Yilmaz, U. Cunedioğli, and E. Baysoy, "Usage of spline interpolation in catheter-based cardiac mapping," *Turkish Journal of Electrical Engineering & Computer Sciences*, vol. 18, no. 6, pp. 989–1002, 2010.

[8] M. Masè and F. Ravelli, "Automatic reconstruction of activation and velocity maps from electro-anatomic data by radial basis functions," in *2010 Annual International Conference of the IEEE Engineering in Medicine and Biology*, 2010, pp. 2608–2611.

[9] S. Coveney, C. Corrado, C. H. Roney, R. D. Wilkinson, J. E. Oakley *et al.*, "Probabilistic interpolation of uncertain local activation times on human atrial manifolds," *IEEE Transactions on Biomedical Engineering*, vol. 67, no. 1, pp. 99–109, 2019.

[10] D. I. Shuman, S. K. Narang, P. Frossard, A. Ortega, and P. Vandergheynst, "The emerging field of signal processing on graphs: Extending high-dimensional data analysis to networks and other irregular domains," *IEEE signal processing magazine*, vol. 30, no. 3, pp. 83–98, 2013.

[11] J. E. Van Engelen and H. H. Hoos, "A survey on semi-supervised learning," *Machine Learning*, vol. 109, no. 2, pp. 373–440, 2020.

[12] M. Belkin, P. Niyogi, and V. Sindhwani, "Manifold regularization: A geometric framework for learning from labeled and unlabeled examples." *Journal of machine learning research*, vol. 7, no. 11, 2006.

[13] M. Hein, J.-Y. Audibert, and U. Von Luxburg, "From graphs to manifolds–weak and strong pointwise consistency of graph laplacians," in *International Conference on Computational Learning Theory*. Springer, 2005, pp. 470–485.

[14] M. Belkin and P. Niyogi, "Towards a theoretical foundation for laplacian-based manifold methods," *Journal of Computer and System Sciences*, vol. 74, no. 8, pp. 1289–1308, 2008.

[15] U. Von Luxburg, "A tutorial on spectral clustering," *Statistics and computing*, vol. 17, no. 4, pp. 395–416, 2007.